Appl Water Sci (2017) 7:1025–1031
DOI 10.1007/s13201-015-0291-1

SHORT RESEARCH COMMUNICATION

Monitoring of ppm level humic acid in surface water using ZnO–chitosan nano-composite as fluorescence probe

Srijita Basumallick[1,4] · **Swadeshmukul Santra**[1,2,3]

Received: 23 February 2015 / Accepted: 21 April 2015 / Published online: 9 May 2015

Abstract Surface water contains natural pollutants humic acid (HA) and fulvic acid at ppm level which form carcinogenic chloro-compounds during chlorination in water treatment plants. We report here synthesis of ZnO–chitosan (CS) nano-composites by simple hydrothermal technique and examined their application potential as fluorescent probe for monitoring ppm level HA. These ZnO–CS composites have been characterized by HRTEM, EDX, FTIR, AFM and Fluorescence Spectra. HRTEM images show the formation of ZnO–CS nano-composites of average diameter of 50–250 nm. Aqueous dispersions of these nano-composites show fluorescence emission at 395 nm when excited at 300 nm which is strongly quenched by ppm level HA indicating their possible use in monitoring ppm level HA present in surface water.

Keywords ZnO nano-rods · Monitoring HA in surface water · Fluorescent probe

✉ Srijita Basumallick
srijitabasumallick@gmail.com

[1] NanoScience Technology Center, University of Central Florida, 12424 Research Parkway, Suite 400, Orlando, FL 32826, USA

[2] Department of Chemistry, University of Central Florida, 12424 Research Parkway, Suite 400, Orlando, FL 32826, USA

[3] Burnett School of Biomedical Sciences, University of Central Florida, 12424 Research Parkway, Suite 400, Orlando, FL 32826, USA

[4] Department of Chemistry, National Institute of Technology, Agartala, India

Introduction

Surface water contains natural organic matter (NOM) in the form of humic acid (HA) and fulvic acid (FA) in the concentration range of 0.1–20 ppm (Rodrigues et al. 2009). Determination of humic substances (HS) such as HA and FA is important in water treatment plant as they form carcinogenic tri-chloro methane-type bi-products (Breider and Albers 2015) during chlorination of water. But estimation of HA using common analytical technique is difficult (Breider and Albers 2015) because of highly heterogeneous structure of HA (Piccolo 2002). Among the spectroscopic techniques, the UV method exploits the UV absorption property of HA at 254 nm (Khan et al. 2014) and IR technique determines the total organic carbon (TOC) using the principle of determination of CO_2 concentration formed after complete combustion of the sample by infrared absorption spectroscopy. But both these techniques suffer from disadvantages such as agglomeration of HA which limits the applicability of Beer's law in UV method and various pre-treatment requirements in TOC method. HA is a major component of HS formed by microbial decomposition of plant bio-mass. Chemically, it has a complex molecular structure (Piccolo 2002) containing both aromatic and aliphatic skeletons with ionisable –COOH and phenolic –OH groups. Because of the presence of these groups, the surface charge of HA colloid is negative (Angelico et al. 2014) (zeta potential is negative at neutral pH). Presence of HA in surface water and water from upland peat catchments in tropical climates is obvious, hence their monitoring and removal are essential prior to their treatment in drinking water plants.

In this communication, we report the preparation of Zn–CS nano-composites and explore the possibility of using these nano-composites as fluorescent probe for estimation

of ppm level HA in surface water intended for drinking purpose. Previously, ZnO nanomaterials (NMs) have been used as (Khayatian et al. 2014) gas sensors. The surface charge of ZnO NMs may be tuned by coating with a positively charged polyelectrolyte as a capping agent.

We report a simple hydrothermal method of synthesis of ZnO nano-composites using depolymerised CS as coating material. CS has been selected as coating material because of two reasons (1) CS is a bio-safe and biodegradable polymer (Saber et al. 2010; Balamurugan 2012) easily obtained from natural polymer chitin; (2) this polyelectrolyte is positively charged (Schatz et al. 2004) at neutral pH, so that CS-capped ZnO will be an ideal material for interacting with negatively charged bio-colloid HA.

During the recent years (Park et al. 2002, Duan et al. 2001 and Huang et al. 2001), much attention has been paid to the synthesis of ZnO NMs such as nano wires, nano belts and nano-rods because of their diverse applications in electronic and photonic devices. Tuning of crystal growth in one direction by chemical synthesis is difficult (Wang et al. 2004) unless some anisotropic force acts in the growth directions. It is reported (Song et al. 2008) that the use of NH_4Cl and Zn salt in alkaline (pH 11.0) hydrothermal synthesis leads to the formation of ZnO nanorods; we have made an attempt to perform similar synthesis of ZnO nanorod–CS composite using acid-depolymerised CS which contains primary amine groups. It is anticipated that the ZnO–CS composites should have positively charged outer surface and will interact with negatively charged HA by electrostatic attraction. It is also anticipated that fluorescence of ZnO–CS composites (Sönmez and Meral 2012) will be quenched upon binding with HA.

Materials and method

Low-molecular weight CS was purchased from Sigma–Aldrich (Saint Louis, Missouri, USA) and used without further treatment. Zinc chloride (technical grade) was purchased from CQ concepts INC (Ringwood, Illinois, USA). Na salt of HA was purchased from Sigma–Aldrich and used as received. Ethanol (95 %) was received from Pharmco-AAPER (Brookfield, CT). ZnO nanomaterials (NMs) were purchased from BASF(Z-COTE® HP1) for using as control.

De-ionized (DI) water was obtained from Barnstead Nanopure Diamond purifier (Model number D11931).

Preparation of depolymerised CS-capped ZnO NPs

300 mg of CS and 300 mg of $Zn(NO_3)_2$ were taken in a hydrothermal tube containing 30 ml 1 % HCl solution and heated to 150 °C for 90 min; at this stage CS underwent depolymerisation and formed complexes with Zn^{2+}. The solution was cooled to room temperature and its pH was adjusted to 11.0 by adding drop by drop 1.0 N NaOH solution in the presence of 100 mg NH_4Cl (Song et al. 2008). The resulting solution was continuously heated at 150 °C under hydrothermal condition as before for 90 min. The solution was cooled and centrifuged at 5000 rpm for 10 min, the precipitate was washed with DI water and the process was repeated 5–6 times to remove unbound chitosan. The final precipitate was vacuum dried for 72 h to obtain powdered product.

HRTEM sample preparation

About 1 mg of ZnO powder sample was dispersed in 1 ml of 95 % (v/v) ethanol using a bath sonicator (Barnstead Lab-Line, model # 9322; 600 Watts). Then a drop of NM suspension was directly placed onto the carbon-coated side of a copper TEM grid. The TEM grid was kept on a piece of Whatman filter paper to absorb excess liquid from the drop. The grid was then air dried for 15 min followed by drying using a vacuum pump overnight.

UV–visible, fluorescence, FTIR and HRTEM studies

UV–vis absorption study was conducted to characterize absorption characteristics of the material to understand interaction of HA with coated ZnO NMs. UV–vis spectra of ZnO–CS composites were recorded using a Varian Cary 300 Bio UV–vis spectrophotometer. Fluorescence excitation and emission measurements of these samples were done using an SPEX Nanolog Spectrofluorimeter (Horiba Jobin–Yvon). Fourier Transform Infra-red Spectroscopy (FT-IR) technique was used to characterize the ZnO NMs and HA-bound NMs. FT-IR spectra were recorded on Perkin Elmer Spectrum 100 attenuated total reflection (ATR) FT-IR Spectrometer. HRTEM was taken with FEI Technai F30 TEM operated at 200 kV.

For AFM images, we used tapping mode operation of the equipment (Veeco Manifold multimode V model) using silicon nitride tip (radius B 50 nm) attached to a cantilever (spring constant = 0.032 Nm, oscillating frequency 0–600 kHz), and the sample was spin coated onto glass surface. All measurements were done at room temperature.

Results and discussions

HRTEM study

Figure 1 shows HRTEM images of CS–ZnO NMs at low magnification (left). Rod-shaped structures are clearly seen. The diameter of the rod is estimated to be

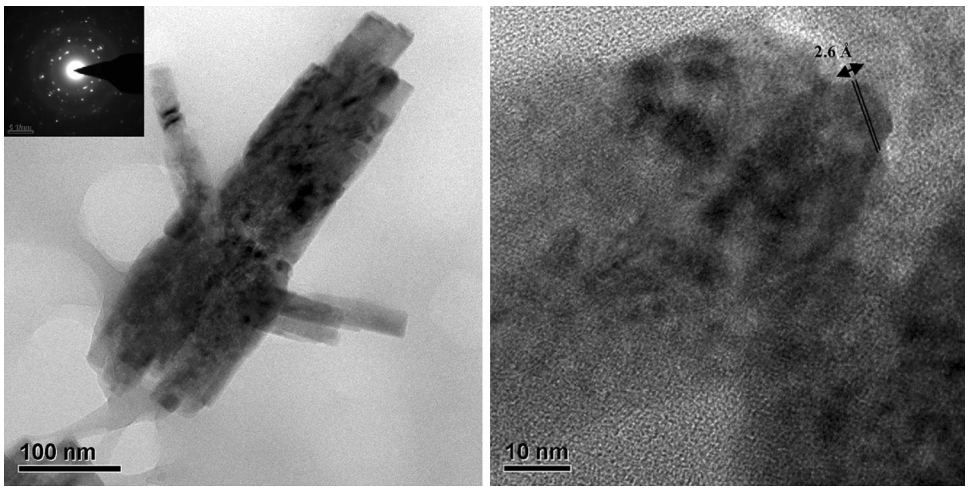

Fig. 1 HRTEM image of ZnO–Chitosan nano-composite under low magnification (*left*), high magnification (*right*) showing *d* spacing 2.6 Å along the growth direction of ZnO nano-rod, Selected area electron diffraction pattern (*left*, *inset*)

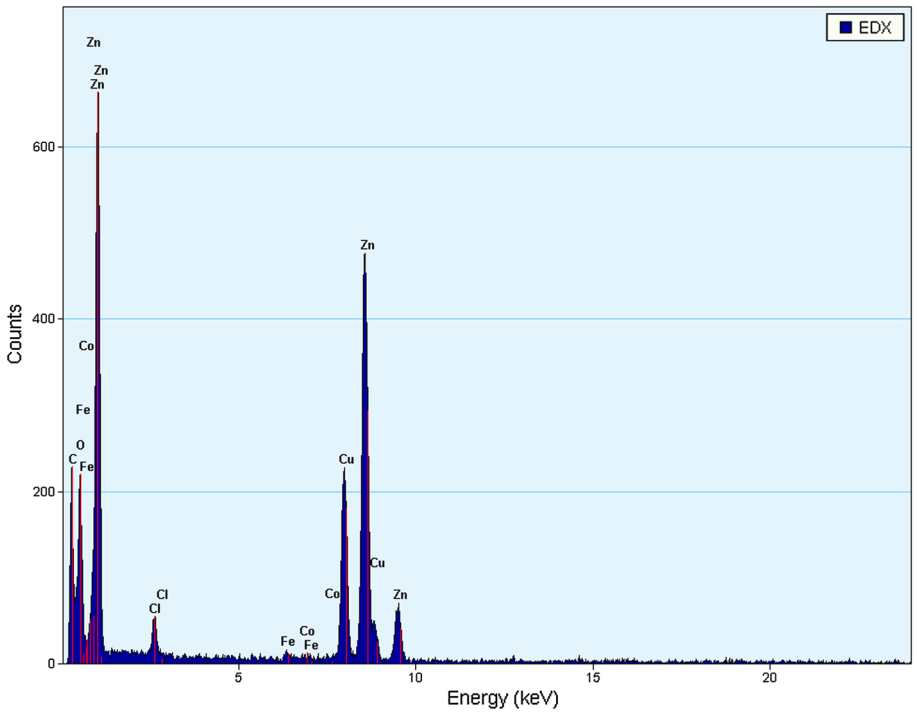

Fig. 2 EDX of ZnO–Chitosan nano-rod

20–25 nm with minimum length of 150–200 nm with an aspect ratio ~8. It is interesting to note that ZnO nano-rods are seen in the form of agglomerated bundle-like structures of thickness about 150 nm and length about 500 nm. This may be due to rapid agglomeration of these NPs coated with depolymerised CS having its cyclic ring structure (Basumallick and Santra 2014). It is reported (Zhang et al. 2013; Hu et al. 2013) that the use of an appropriate capping agent can tune the crystal shape. Weak capping agent promotes (Zhang et al. 2013) lateral stacking of ZnO nano-rods as we observed in our case. ZnO–CS composites along with some black patch on the ZnO nano-rods are seen in the TEM images. Apart from growth in the vertical direction, branching is also noticed in horizontal direction. This type of branching during crystal growth has been explained by Kirkpatrick (1975) and (Tan et al. 2013). The HRTEM—selected area diffraction pattern (SAED), in Fig. 1 inset, shows a strong electron diffraction pattern, confirming the presence of a crystalline ZnO core with no definite shell structure. Higher magnification (Fig. 1, right) image shows ZnO nano-rods with d spacing of 2.6 Å for (0002) planes are

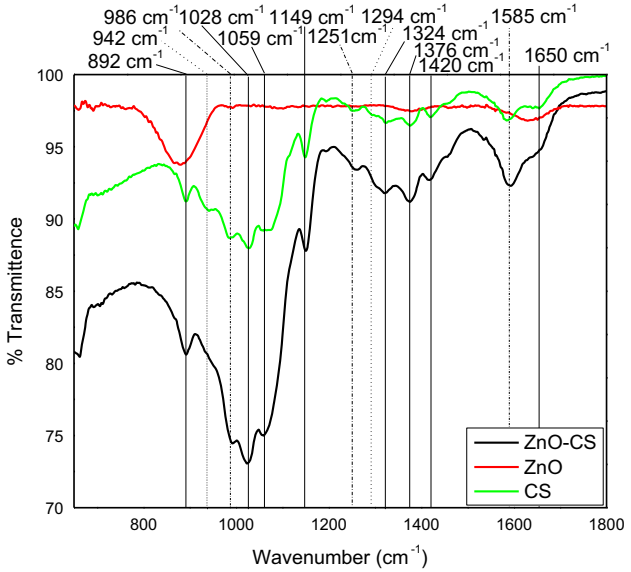

Fig. 3 FT-IR spectra of ZnO–Chitosan nano-composite (*black line*), ZnO control (*red line*), Chitosan control (*green line*)

embedded by chitosan film. Bright spots in SAED (selected area electron diffraction pattern) indicate the formation of pure crystal as well as the branching of the crystals reinforces the purity. It is known that the positive polar surface (0001) is more thermodynamically favourable (Tan et al. 2013) for rod-like crystal growth. The negative polar surface (000-1) on the other hand can bind to the cationic capping agent like CS and act as possible nucleation growth site for another direction leading to branching (Kirkpatrick 1975). It is known that (0001) face is efficient in sensing applications of ZnO (Ludi et al. 2012; Kaneti et al. 2014), the branched as well as the stacked nano-rods have their crystal structures with (0001) planes retained. Purity of prepared ZnO–CS nano-rods has been confirmed from EDX analysis (Fig. 2); appearance of small Fe peaks are coming from the steel holder.

FTIR study

Chitosan and chitosan-coated ZnO nano-rod have more or less similar IR peaks, whereas ZnO control (prepared without CS) has no peaks assigned for CS capping agent. Control ZnO particles show a peak around 1650 cm^{-1} corresponding to carbonyl stretching frequency that is overlapped with the chitosan peak in the chitosan-coated ZnO nano-rod composites. The major change seen in N–H stretching (1585 cm^{-1}) (Kumirska et al. 2010) and $–CH_2$ twisting and bending [1294 cm^{-1} (Dai et al. 2005); 1251 cm^{-1}] indicates the interaction of ZnO with N–H group as well as aliphatic part of chitosan. Observed shifts of N–H and C–H stretching as seen with CS-coated ZnO nano-rod may be due to interactions of ZnO with –NH/–CH of CS. Other than that, change in peaks at 942 and 986 cm^{-1} might indicate interaction and deformation of chitosan skeleton (Leceta et al. 2013). But the peak at 1149 cm^{-1} remained the same indicating no major change in glycoside linkage. Among other important peaks at 1420, 1376 and 1324 cm^{-1} corresponding to primary alcohol (–OH plane deformation) (Leceta et al. 2013), CH_3 symmetric deformation (Leceta et al. 2013) and C–N of amide band (Fernandes et al. 2013) remained intact (Fig. 3).

AFM study

AFM images of Zno–CS composite are shown in Fig. 4. It is seen that ZnO nano-particles are covered with CS coatings and the particles are to some extent agglomerated. It is also seen larger size agglomerates are formed from smaller-sized particles which are around 332 nm.

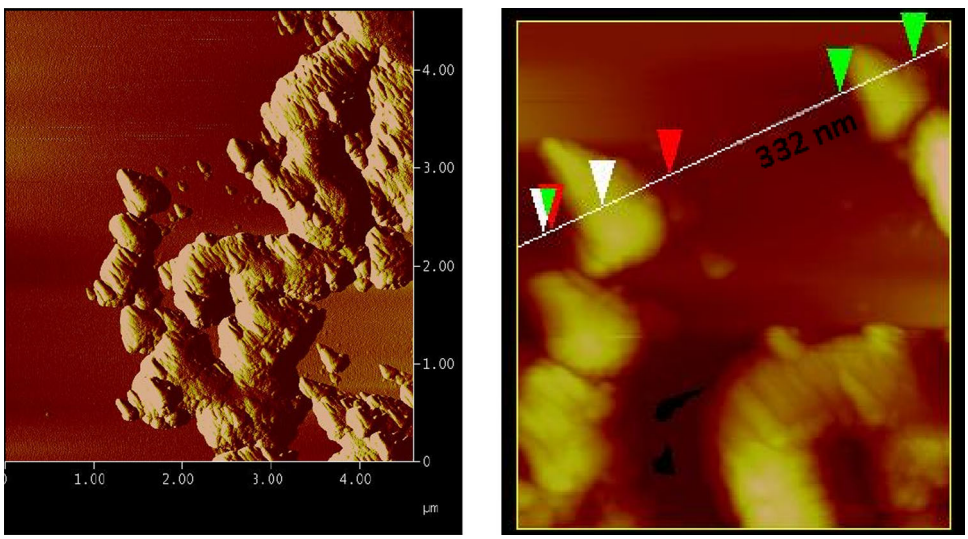

Fig. 4 AFM image of ZnO–Chitosan nano-composites and their dimensions (*right*)

Fluorescence study

The UV–Vis absorption shows an absorption peak at 380 nm characteristic to ZnO band gap. The fluorescence emission spectra of ZnO–CS NMs are shown in Fig. 5, at an excitation wavelength of 300 nm. It shows an emission peak around 395 nm that is attributed to the band edge spectra of ZnO–CS NMs and a small shoulder peak at ~376 nm corresponding to that of uncoated ZnO nano-crystals. The observed red shift for CS-coated ZnO NMs may be due to polar environment provided by highly hydrophilic CS. Fluorescence spectra of ZnO NMs have been studied (Panigrahi et al. 2011; Iripman et al. 2007) extensively by other researchers, apart from its excitation wavelength dependent of emission spectra it shows green or visible emission around 500 nm due to surface defects. The latter emission is not very prominent here.

It is interesting to note that fluorescence intensity of ZnO–CS is gradually quenched by HA till 24 ppm of HA concentration; the observed fluorescence quenching primarily indicates interactions of ZnO–CS with HA.But above this concentration of HA, no further quenching is noticed. This may be owing to completion of monolayer coverage of HA (Röcker et al. 2009) onto ZnO–CS surface.

For the sake of comparison, we performed similar experiment with ZnO NMs purchased from BASF and its fluorescence spectra and quenching behaviour with HA is shown in Fig. 6. The emission peak appears at 390 nm, the observed red-shift with ZnO–CS is attributed to the more hydrophilic environment provided by CS coating onto ZnO surface. It is interesting to note that here fluorescence quenching starts at a very high concentration of HA (1.2 mg/ml).

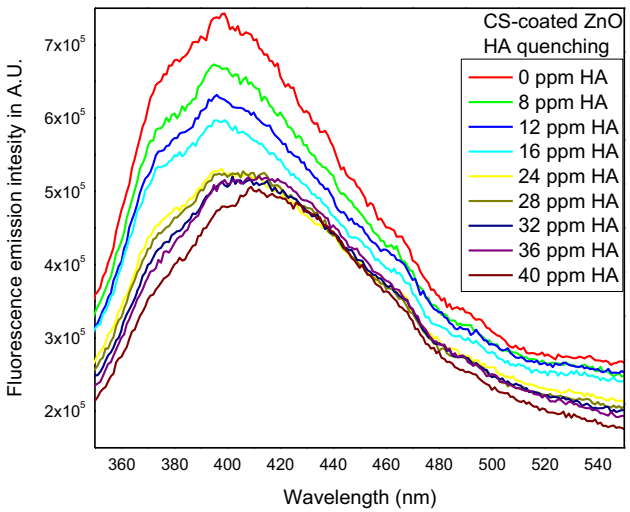

Fig. 5 Quenching of ZnO–Chitosan nano-composite fluorescence by HA (*inset*; from 8 to 40 ppm) ($\lambda_{ex} = 300$ nm)

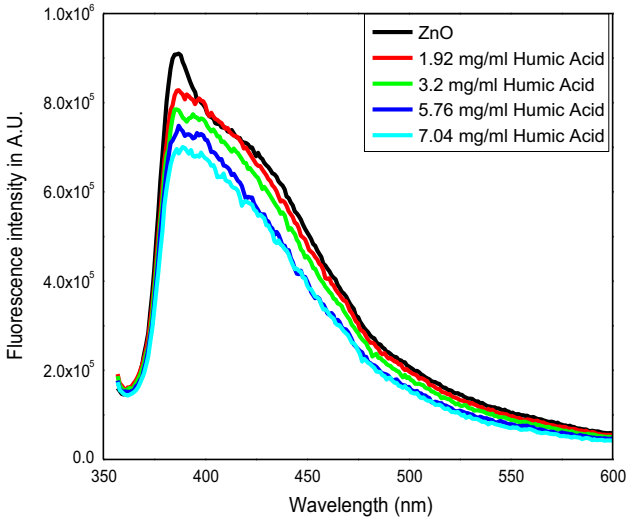

Fig. 6 Quenching of ZnO NMs (without CS) fluorescence by HA (*inset*; from 1.92 to 7.04 mg/ml)

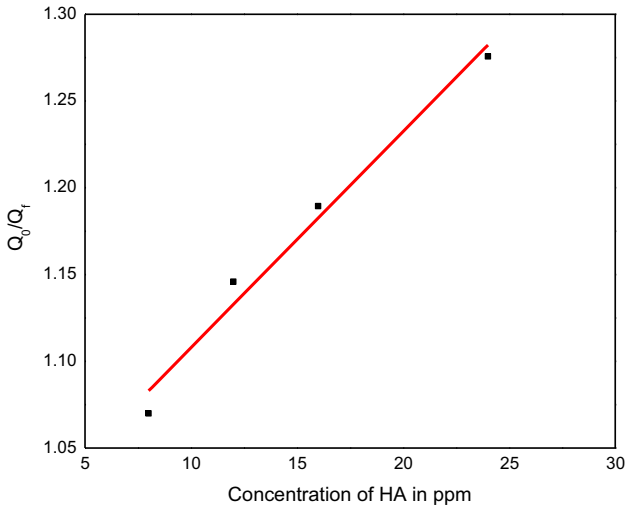

Fig. 7 Stern–Volmer plot with HA as quencher for ZnO–CS fluorescence up to 24 ppm

HA adsorption onto inorganic metal oxides including ZnO has been reported earlier (Yang et al. 2009), but its adsorption onto bio-polymer-coated ZnO nano-rod has not been studied earlier. To understand the basic nature of this interaction, we have made an analysis of the FTIR spectra of CS-ZnO (Fig. 3). FTIR spectra do not indicate any chemical bond formation between CS and surface ions of ZnO nano-crystals. Thus, CS, a positively charged polyelectrolyte (even at neutral pH binds to ZnO and HA by electrostatic interactions). Recently, the importance of electrostatic interaction in binding process of humic acid onto ZnO nano-particle surface has been reported by Stoll et al. (2013). Earlier almost similar conclusions were proposed by Rabani and Behar (1989) from their study on ZnO

colloids with poly-electrolytes of different charges. Stern–Volmer plot of fluorescence quenching by HA is shown in Fig. 7 that clearly shows linear curve and enables estimation of HA within this concentration range. Since ZnO–CS fluorescence is quenched by HA appreciably at very low (ppm) concentrations, development of an easy and cost-effective technique for the estimation of ppm level HA in surface water is indicated from this preliminary study.

Conclusions

In conclusion, we have synthesized water-dispersible ZnO–CS nano-composites by simple hydrothermal method and demonstrated that these NMs may be used as fluorescence sensors for the estimation of ppm level HA with estimation limit up to 24 ppm. This preliminary result indicates possible applicability of this technique in the estimation of HA in water treatment plants.

Acknowledgments The authors are thankful to the Reviewers for their valuable suggestions. SBM is thankful to Professor S Seal, Director of NSTC, UCF for support and encouragement.

References

Angelico R, Ceglie A, He JZ, Liu YR, Palumbo G, Colombo C (2014) Particle size, charge and colloidal stability of HAs coprecipitated with Ferrihydrite. Chemosphere 99:239–247

Balamurugan M (2012) Chitosan: a perfect polymer used in fabricating gene delivery and novel drug delivery systems. Int J Pharm Pharm Sci 4(3):54–56

Basumallick S, Santra S (2014) Chitosan coated copper-oxides nanoparticles: a novel electro-catalyst for CO_2 reduction. RSC Adv 4:63685–63690

Breider F, Albers CN (2015) Formation mechanisms of trichloromethyl-containing compounds in the terrestrial environment: a critical review. Chemosphere 119:145–154

Dai S, Zhanga X, Dua Z, Huanga Y, Danga H (2005) Structural properties and Raman spectroscopy of lipid Langmuir monolayers at the air–water interface. Coll Surf B Biointerfaces 42:21–28

Duan X, Huang Y, Cui Y, Wang J, Lieber CM (2001) Indium phosphide nanowires as building blocks for nanoscale electronic and optoelectronic devices. Nat Lond 409:66–69

Fernandes M, Goncalves IC, Nardecchia S, Amaral IF, Barbosa MA, Martins MCL (2013) Modulation of stability and mucoadhesive properties of chitosan, microspheres for therapeutic gastric application. Int J Pharm 454:116–124

Hu Q, Tong G, Wu W, Liu F, Qian H, Hong D (2013) Selective preparation and enhanced microwave electromagnetic characteristics of polymorphous ZnO architectures made from a facile one-step ethanediamine-assisted hydrothermal approach. CrystEngComm 15:1314–1323

Huang MH, Mao S, Feick H, Yan H, Wu Y, Kind H, Weber E, Russo R, Yang P (2001) Room-temperature ultraviolet nanowire nanolasers. Science 292(5523):1897–1899

Iripman L, Nampuri VPN, Rudhrakrishnan P, Deepthy A, Krishnan BJ (2007) Size dependent fluorescence spectroscopy of nanocolloids of ZnO. Appl Phys 102:063524–063526

Kaneti YV, Zhang Z, Yue J, Zakaria QMD, Chen C, Jiang X, Yu A (2014) Crystal plane-dependent gas-sensing properties of zinc oxide nanostructures: experimental and theoretical studies. Phys Chem Chem Phys 16:11471–11480

Khan S, Yaoguo W, Xiaoyan Z, Youning X, Jianghua Z, Sihai H (2014) Estimation of concentration of dissolved organic matter from sediment by using UV–visible spectrophotometer. Int J Environ Pollut Remediat 2(1):24–29

Khayatian A, Kashi MA, Azimirad R, Safa S (2014) Enhanced gas-sensing properties of ZnO nanorods encapsulated in an Fe-doped ZnO shell. J Phys D Appl Phys 47:075003

Kirkpatrick RJ (1975) Crystal growth from the melt: a review. Am Mineral 60:798–814

Kumirska J, Czerwicka M, Kaczyński Z, Bychowska A, Brzozowski K, Thöming J, Stepnowski P (2010) Application of spectroscopic methods for structural analysis of chitin and chitosan. Mar Drugs 8:1567–1636

Leceta I, Guerrero P, Ibarburu I, Duenas MT, de la Caba K (2013) Characterization and antimicrobial analysis of chitosan-based films. J Food Eng 116:889–899

Ludi B, Süess MJ, Werner IA, Niederberger M (2012) Mechanistic aspects of molecular formation and crystallization of zinc oxide nanoparticles in benzyl alcohol. Nanoscale 4:1982–1995

Panigrahi S, Bera A, Basak D (2011) Ordered dispersion of ZnO quantum dots in SiO_2 matrix and its strong emission properties. J Coll Interface Sci 353(1):30–38

Park WI, Kim DH, Jung SW, Yia GC (2002) Metalorganic vapor-phase epitaxial growth of vertically well-aligned ZnO nano rods. Appl Phy Lett 80:4232–4234

Piccolo A (2002) The supramolecular structure of humic substances: a novel understanding of Humus chemistry and implications in soil science. Adv Agron 75:57–134

Rabani J, Behar D (1989) Quenching of aqueous colloidal ZnO fluorescence by electron and hole scavengers. Effect of a positive polyelectrolyte. J Phys Chem 93:2559–2563

Röcker C, Pötzl M, Zhang F, Parak WJ, Nienhaus GU (2009) A quantitative fluorescence study of protein monolayer formation on colloidal nanoparticles. Nat Nanotechnol 4:577–580

Saber A, Strand SP, Ulfendahl M (2010) Use of the biodegradable polymer chitosan as a vehicle for applying drugs to the inner ear. Eur J Pharm Sci 39:110–115

Schatz C, Lucas JM, Viton C, Domard A, Pichot C, Delair T (2004) Formation and properties of positively charged colloids based on polyelectrolyte complexes of biopolymers. Langmuir 20(18):7766–7778

Song J, Baek S, Lee J, Lim S (2008) Role of OH^- in the low temperature hydrothermal synthesis of ZnO nanorods. J Chem Technol Biotechnol 83(3):345–350

Sönmez E, Meral K (2012) Enhancement of photoluminescence lifetime of ZnO nanorods making use of thiourea. J Nanomater 6:1–6

Stoll S, Abdul AH, Mohd AF (2013) Aggregation and disaggregation of ZnO nanoparticles: influence of pH and adsorption of Suwannee River humic acid. Science of the total environment 468–469C: 195–201. doi:10.1016/j.scitotenv.2013.08.044

Tan ST, Umar AA, Yahaya M, Salleh MM, Yap CC, Nguyen HQ, Dee CF, Chang EY, Oyama M (2013) Formation of a multi-arm

branched nanorod of ZnO on the Si surface via a nanoseed-induced polytypic crystal growth using the hydrothermal method. Sci Adv Mater 5:1–7

Wang X, Summers CJ, Wang ZL (2004) Large-scale hexagonal-patterned growth of aligned ZnO nanorods for nano-optoelectronics and nanosensor arrays. Nano Lett 4(3):423–426

Yang K, Lin D, Xing B (2009) Interactions of HA with nanosized inorganic oxides. Langmuir 25(6):3571–3576

Zhang RH, Slamovich EB, Handwerker CA (2013) Controlling growth rate anisotropy for formation of continuous ZnO thin films from seeded substrates. Nanotechnology 17(24):195603–195700